LETTERS
PUBLISHED ONLINE: 20 OCTOBER 2013 | DOI: 10.1038/NNANO.2013.206
nature nanotechnology

Graphene–MoS_2 hybrid structures for multifunctional photoresponsive memory devices

Kallol Roy[1]*, Medini Padmanabhan[1], Srijit Goswami[1†], T. Phanindra Sai[1], Gopalakrishnan Ramalingam[2†], Srinivasan Raghavan[2] and Arindam Ghosh[1]*

Combining the electronic properties of graphene[1,2] and molybdenum disulphide (MoS_2)[3–6] in hybrid heterostructures offers the possibility to create devices with various functionalities. Electronic logic and memory devices have already been constructed from graphene–MoS_2 hybrids[7,8], but they do not make use of the photosensitivity of MoS_2, which arises from its optical-range bandgap[9]. Here, we demonstrate that graphene-on-MoS_2 binary heterostructures display remarkable dual optoelectronic functionality, including highly sensitive photodetection and gate-tunable persistent photoconductivity. The responsivity of the hybrids was found to be nearly 1×10^{10} A W^{-1} at 130 K and 5×10^{8} A W^{-1} at room temperature, making them the most sensitive graphene-based photodetectors. When subjected to time-dependent photoillumination, the hybrids could also function as a rewritable optoelectronic switch or memory, where the persistent state shows almost no relaxation or decay within experimental timescales, indicating near-perfect charge retention. These effects can be quantitatively explained by gate-tunable charge exchange between the graphene and MoS_2 layers, and may lead to new graphene-based optoelectronic devices that are naturally scalable for large-area applications at room temperature.

Sensitizing graphene-based field-effect devices to optical excitation can have a strong impact on technologies ranging from photodetection and photovoltaics to optical modulators and high-speed data communication. The emphasis so far has been predominantly on photodetection and improving the optical responsivity, γ, of graphene[10–20], and other optoelectronic effects such as persistent photoconductivity (PPC), where electromagnetic excitation shifts the electrical resistance of the host material to a slowly relaxing state, have received far less attention. Although PPC is traditionally observed in compound semiconductors, alloys and heterojunctions[21–23], such an effect in graphene phototransistors would readily benefit from strong coupling to light over a wide band of wavelengths[24,25], high carrier mobility[2], gate tunability, miniaturization and the ability to pattern over a large area. However, available reports of PPC in suspended graphene[15] or graphene–nanoparticle composites[26] suffer either from uncontrolled environmental effects or short persistence times.

The intrinsic optical responsivity of graphene is usually poor ($\gamma \leq 1 \times 10^{-2}$ A W^{-1}) (refs 10–12). This has led to composite or hybrid structures containing graphene that enhance carrier multiplication, or gain, by generating multiple charge carriers with a single photon[26–28]. Such hybrid structures are naturally suited for PPC, because the photogenerated carriers are created externally, such as in quantum dots[26] or chromophores[27], and then transferred to graphene via electrostatic bending of the bands. The physical separation of the electrons and holes by the interfacial barrier leads to long recombination time ($\tau_{lifetime}$) in comparison to the transit time ($\tau_{transit}$) of carriers through graphene. Although this has resulted in large photoresponsivity, to date the PPC in graphene hybrids has been weak and time-limited to a few tens of seconds.

Being layered semiconductors, several members of the transition-metal dichalcogenide (TMDC) family, particularly MoS_2 and WS_2, make natural partners to graphene for optically active heterostructures. Strong optical absorption (1×10^{7} m^{-1}) and a visible-range bandgap (1.9 eV and 1.2 eV for single- and multilayer MoS_2, respectively[9]) allow an exceptional photoresponse in graphene–TMDC heterostructures, with large quantum efficiency and photocurrent generation[29]. Because the TMDC can be mechanically exfoliated down to single molecular layers, ultrathin binary or multilayered heterostructures with trap-free interfaces can be formed with a non-invasive physical attachment that preserves the high carrier mobility in graphene, while facilitating easy exchange of charge across the interface under the influence of external electric fields. The uniqueness of MoS_2, in addition to its field-effect properties, lies in the field-dependent nature of its electronic states, which can be tuned from localized to extended regimes with the gate voltage[4]. In this Letter, we show that this tunability, assisted by the graphene-on-MoS_2 stacking sequence, allows a new class of optoelectronic design that not only exhibits a gigantic photoresponse, but can also facilitate the creation of programmable charge storage devices.

A typical device architecture is shown in Fig. 1a and a representative scanning electron microscopy (SEM) image in the inset. We overlayed single-layer graphene on a multilayer MoS_2 flake, with the latter placed on a Si/SiO_2 substrate with thickness varying from 2 to 10 molecular layers (see Methods for details). The fabrication technique is the same as that for overlaying exfoliated graphene on BN microflakes, and provides a trap-free high-quality interface[2,30]. As a result, carrier mobility μ as high as $\sim 1 \times 10^{4}$ cm^2 V^{-1} s^{-1}, could be achieved in our graphene devices, which plays a crucial role in enhancing the gain under photoillumination.

Figure 1b presents the source–drain current I_{ds} between contacts located on the graphene as a function of backgate voltage V_g for a typical graphene–MoS_2 hybrid device in which the MoS_2 flake contains approximately five molecular layers ($T = 130$ K and source–drain bias $V_{ds} = 0.1$ V). Even in the absence of light (black trace in Fig. 1b), the $I_{ds} - V_g$ data were found to be very different from the usual 'bell-shaped' gate characteristics of graphene on insulating substrates such as SiO_2. The saturation of I_{ds} with increasing V_g can be understood by correlating with the gate characteristics

[1]Department of Physics, Indian Institute of Science, Bangalore 560012, India, [2]Centre for Nano Science and Engineering and Materials Research Center, Indian Institute of Science, Bangalore 560012, India, †Present address: Kavli Institute of Nanoscience, Delft University of Technology, PO Box 5046, 2600 GA Delft, The Netherlands (S.G.); Department of Materials Science and Engineering, University of Virginia, Charlottesville, Virginia 22904, USA (G.R.). *e-mail: kallol@physics.iisc.ernet.in; arindam@physics.iisc.ernet.in

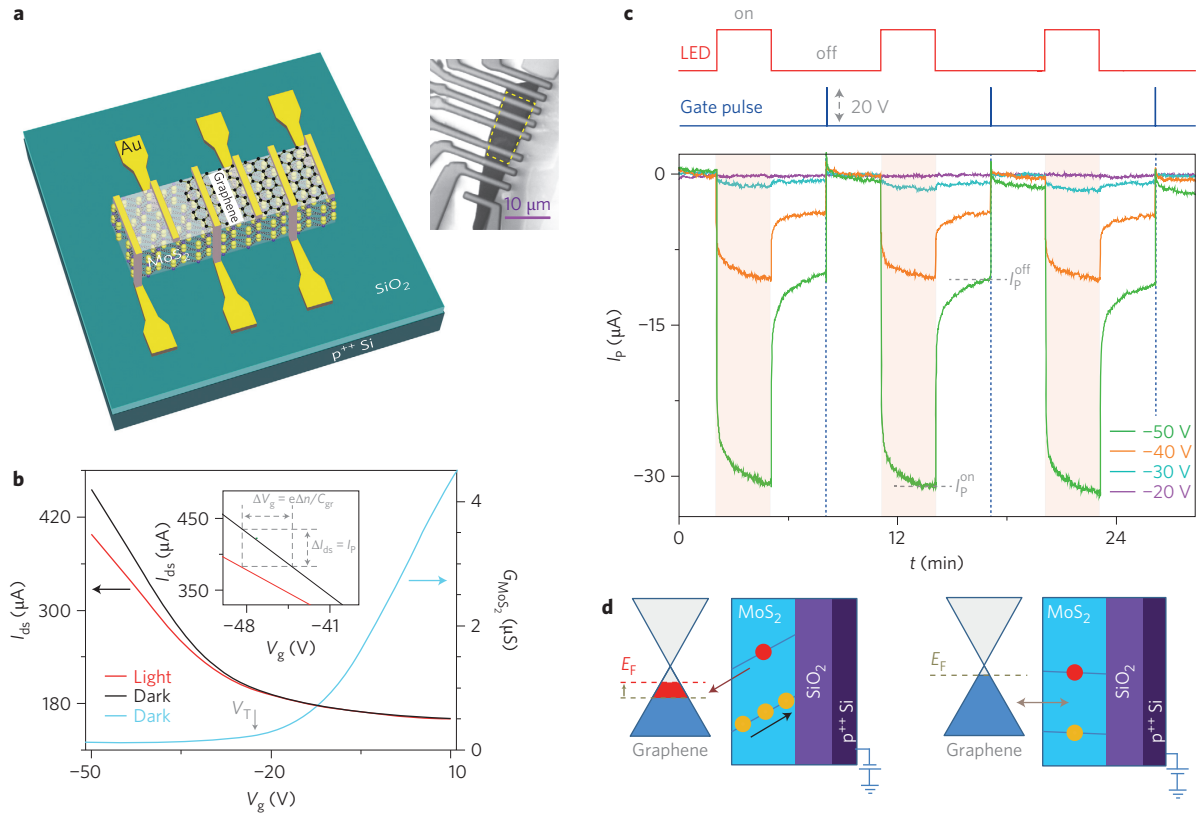

Figure 1 | Device and optoelectronic response. a, Schematic of device architecture. Inset: SEM image of a typical device. The dotted line indicates the outline of the graphene. **b**, Black and red solid lines: source–drain current (I_{ds}) versus backgate voltage (V_g) for graphene on MoS_2 in the absence and presence of light, respectively. Cyan coloured trace: V_g-dependent conductance of bare MoS_2 in the dark. **c**, Gate voltage-dependent photocurrent induction and switching operation. Vertical shaded columns and blue (dotted) lines indicate the presence of light and application of gate pulses, respectively. **d**, Schematic of charge exchange process for $V_g \ll V_T$ (left panel) and positive V_g ($>V_T$) (right panel). Red and yellow circles represent electrons and holes in the conduction and valence bands of MoS_2, respectively.

of the underlying MoS_2 (cyan trace). Being n-type in nature, the MoS_2 channel begins populating only for $V_g \geq V_T$ and screens the backgate from graphene (here V_T is the MoS_2 conduction threshold). Typically, V_T lies between -10 V and -30 V for most multilayer MoS_2 channels that we have measured[4], which explains the absence of the Dirac point (V_D) for the device in Fig. 1b for which $V_T < V_D$.

The device was then illuminated with a red light-emitting diode (LED, wavelength = 635 nm) at a photoexcitation intensity (P_{LED}) of 376 fW μm^{-2}. The red trace in Fig. 1b represents the variation of I_{ds} with V_g when the device was illuminated continuously. Note that there is a pronounced effect at $V_g \ll V_T$, where graphene is heavily hole-doped and MoS_2 forms a strongly insulating underlayer. A decrease in I_{ds} is observed in the presence of light, where the absolute magnitude of the photocurrent I_P increases as V_g is made more negative, but reduces to ~0 for $V_g > V_T$. The negative sign of the photoconductivity can be easily understood from the transfer of the photoelectrons generated inside MoS_2 to the graphene under the influence of negative V_g (see schematic in Fig. 1d, left panel). Because graphene is hole-doped, the addition of electrons increases its resistance R, thereby decreasing I_{ds}. The bands in MoS_2 stay flat because of its near-metallic nature when $V_g \geq V_T$, suppressing the unidirectional transfer of electrons, and equilibrating the charge distribution throughout the hybrid (Fig. 1d, right panel).

In Fig. 1c we show the result of three photoillumination cycles. On turning the LED on, $-I_P$ increases sharply and saturates at a V_g-dependent magnitude I_P^{on} within a few seconds. However, switching the light off does not remove the photocurrent completely; instead it saturates to a new (smaller) magnitude I_P^{off}, indicating long-term negative PPC. The pre-illumination state ($I_P = 0$) could be recovered only by a gate voltage pulse that elevates the Fermi energy momentarily to ~V_T, thereby equilibrating the charge distribution. Both I_P^{on} and I_P^{off} increase rapidly as V_g is made more negative for fixed illumination power, indicating that the graphene–MoS_2 hybrids can be designed to function as versatile gate-tunable photodetectors as well as optoelectronic switches.

To evaluate the responsivity γ of the hybrids, we focus on I_P^{on}, which depends linearly on V_{ds} at low biases ($\leq$0.05 V), but becomes sublinear at higher bias (Fig. 2a). The variation of I_P^{on} is weak for LED power $P_{LED} \geq 10$ fW μm^{-2} (Fig. 2c, top-right inset), which can be attributed to lowering of the in-built electric field due to a large accumulation of photogenerated carriers[26]. The responsivity calculated from $\gamma = I_P/P_{LED}$ at $V_{ds} = 0.1$ V was found to reach an extremely large value $\gamma \approx 1 \times 10^{10}$ A W^{-1} at a low excitation intensity ($P_{LED} = 1$ fW μm^{-2}) and $T = 130$ K (Fig. 2c). The bottom-left inset of Fig. 2c compares the V_g dependence of γ at 130 K and room temperature for a slightly higher photoexcitation power ($P = 6.4$ fW μm^{-2}). Under these conditions, a room-temperature responsivity of $\sim 5 \times 10^8$ A W^{-1} was achieved at $V_g = -50$ V (before the gate started leaking), exceeding the responsivity of graphene–nanoparticle hybrids by a factor of ~10 (ref. 26).

The large γ implies a high gain (~4×10^{10} at low T, Supplementary Section S6), which can be verified from the quantum efficiency η, recombination lifetime $\tau_{lifetime}$ and carrier mobility μ. We estimated $\eta \approx 0.3$ from the change in doping of the graphene following illumination with a known photon flux (see Methods). The relaxation of I_P with change in

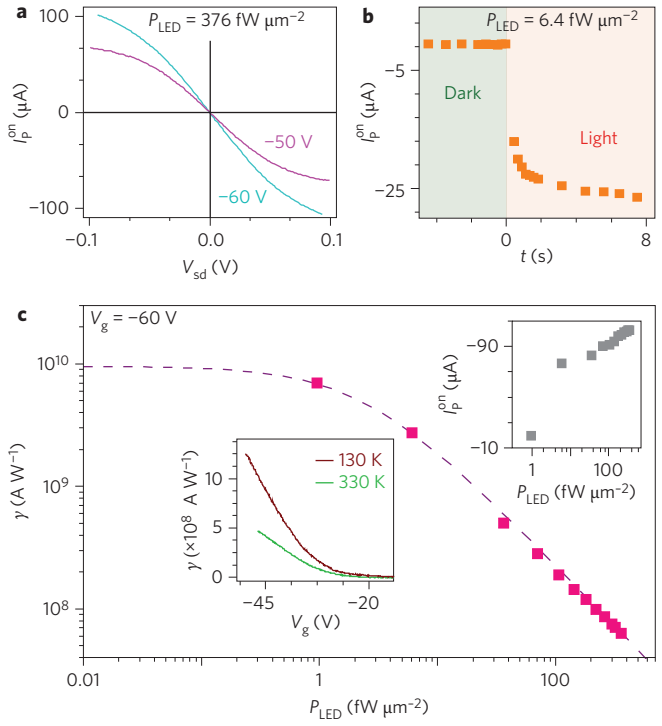

Figure 2 | Photoresponsivity of graphene–MoS_2 hybrid. a, Dependence of I_P^{on} on source–drain bias V_{ds} at two different gate voltages ($\lambda = 635$ nm, $P_{LED} = 376$ fW μm^{-2}). **b**, Time trace of photocurrent on light illumination at $V_g = -50$ V. **c**, Responsivity γ as a function of illumination power. Dashed line is a fit of the form $A_1/(A_2 + P_{LED})$, considering A_1 and A_2 as the fitting parameters. Top-right inset: change in I_P^{on} ($V_{ds} = 0.1$ V) with LED power. Bottom-left inset: comparison of low-temperature and room-temperature responsivity.

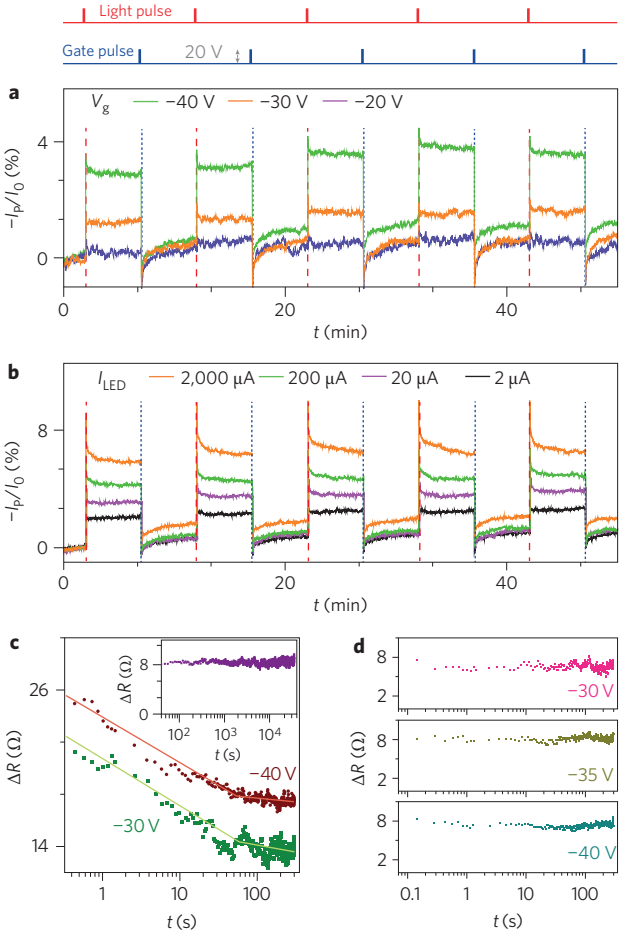

Figure 3 | Gate- and intensity-dependent switching and relaxation. a, Evolution of the switching effect as a function of V_g. For all traces, $I_{LED} = 10$ μA. **b**, Switching with different light intensities at $V_g = -40$ V. **c**, Transition from logarithmic decay to nearly relaxation-free state after photoexcitation with an LED current of 200 μA for 0.1 s. Solid lines are guides to the eye. Inset: persistent state over a long timescale (~12 h). **d**, Nearly relaxation-free nature of persistent states at three different gate voltages.

photoexcitation estimates $\tau_{lifetime}$ to be ~1 s (Fig. 2b), although at long times the relaxation often becomes logarithmic. Thus, using $\mu \approx 1 \times 10^4$ cm^2 V^{-1} s^{-1}, we obtain a gain of $\sim 5 \times 10^{10}$–10×10^{10}, in good agreement with the experimental result. The trap-free heterojunctions in the graphene–MoS_2 hybrids play key roles in enhancing the responsivity, by allowing (1) larger carrier mobility (and hence a low transit time) in graphene and (2) unhindered transfer of the photogenerated electrons from MoS_2 to graphene under the gate electric field.

The PPC was investigated in more detail in a different device with approximately the same thickness of MoS_2 ($V_T \approx -10$ V, $V_D = -8$ V), and is illustrated in Fig. 3. To focus on the time evolution of I_P^{off} and also to demonstrate the switching action, we used pulsed illumination from a white LED (pulsewidth ~0.1 s) where the illumination intensity is represented by the current I_{LED} used to excite the LED (when $I_{LED} = 5$ mA, $P_{LED} \approx 50$ pW μm^{-2}). Within the experimental range of I_{LED}, I_P^{off} as large as ~5% of the pre-illumination current (I_0) was observed in the strongly hole-doped regime and at low temperatures ($T = 110$ K, Fig. 3a). As expected, the illumination has no measurable effect when V_g approaches V_T. The 'light set–voltage reset' cycles could be performed over days with better than 95% accuracy in recovering the persistent state current. I_P^{off} could also be tuned by the photoexcitation intensity, which not only affects the overall magnitude of I_P^{off}, but also the nature of its relaxation in time (Fig. 3b). For stronger illuminations ($I_{LED} > 50$ μA) the relaxation is initially ($t \leq 100$ s) logarithmic, but becomes nearly constant at longer times. This is shown in Fig. 3c by the relaxation of persistent state resistance following a 200 μA pulse. Almost no relaxation was observed for low I_{LED} (≤20 μA), implying almost perfectly non-volatile charge retention. The non-volatility was found irrespective of the gate voltage, even though the absolute magnitude of I_P^{off} may differ (Fig. 3d), and remains unchanged over the maximum duration used in our experiments (exceeding 12 h, inset of Fig. 3c, $I_{LED} = 5$ μA for 30 ms).

Our control experiments with either MoS_2 or isolated graphene show no evidence of PPC, implying that the observed phenomenon is an intrinsic property of the hybrids (Supplementary Section S2). Assemblies of carbon-based nanomaterials, in particular composites of carbon nanotube and light-absorbing polymers, have also displayed the external tunability of the PPC (refs 31–34). The finite I_P^{off} in these devices has been attributed to the presence of a gate electric field that resists electron–hole recombination. However, the PPC in our case is a combined effect of carrier localization in MoS_2 (ref. 4) and the directionality of the gate electric field (schematic in Fig. 4a). The former can naturally lead to a logarithmic relaxation in PPC (ref. 23), as seen for strong illumination and shorter times (Fig. 3c). To verify this quantitatively for our case, we used the V_g dependence of I_P^{off} (Fig. 4b, top-left inset), and calculated the excess electron density in graphene from the gate-voltage shift ΔV_g in the persistent state (Fig. 1b, inset). Assuming an activated recombination probability and linear band structure

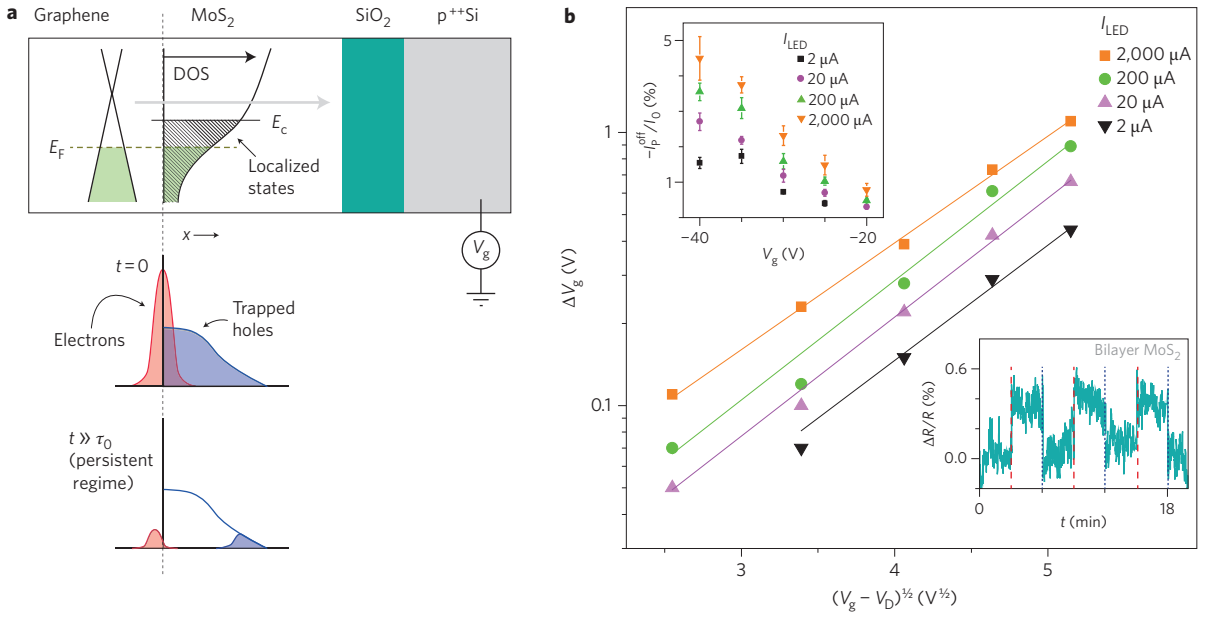

Figure 4 | Persistent photoconductivity mechanism. a, Schematic showing evolution of the electron–hole distribution in the system as a function of time. $t = 0$ corresponds to application of the light pulse. The light grey arrow indicates the direction of the electric field for negative gate voltages. **b**, Effective gate voltage shift (ΔV_g) versus $\sqrt{V_g - V_D}$. Top-left inset: percentage change in photocurrent I_P as a function of V_g. Error bars are calculated from measurements in multiple cycles. Bottom-right inset: illustration of the switching cycles of a graphene–MoS_2 device, where the MoS_2 is two layers thick.

for graphene, ΔV_g can be expressed as (see Supplementary equation (S9) and Supplementary Section S3 for detailed derivation)

$$\Delta V_g \propto \exp[\beta\sqrt{|V_g - V_D|}]$$

where $\beta = \hbar v_F\sqrt{(\pi C_{gr}/e)}/k_B T$. Here, C_{gr} is the effective capacitance between the silicon backgate and graphene, and v_F is the Fermi velocity in graphene. The exponential increase in ΔV_g with $|V_g - V_D|^{1/2}$ is clearly observed for different intensities of photoexcitations in Fig. 4b. Experimentally, we obtain $\beta \approx 1.1$, which is within a factor of approximately two of the theoretically expected β for a 285 nm SiO_2 dielectric.

The deviation from the logarithmic relaxation at longer times, as well as the non-volatility under low-intensity illumination, can be attributed to the potential barrier (~0.8 eV for a 5 nm MoS_2 film at $V_g = -50$ V) to electron–hole recombination arising from the graphene-on-MoS_2 device architecture. Unlike the graphene–nanoparticle hybrids[26], where the light-sensitive nanoparticles were placed on the exposed surface of the graphene, thereby eliminating any significant effect from the gate electric field on charge exchange, the present arrangement allows greater operational versatility allowing, for example, inverted stacking or multilayers. The importance of the electric field-induced barrier can be readily observed in the strong suppression of both photoresponsivity and PPC (to <0.5% at 130 K) when the number of layers in MoS_2 is reduced to two, that is, to a thickness of ~1.5 nm (Fig. 4b, bottom-right inset). This also eliminates any role of impurities or surface contamination in the observed photoresponse. Additional effects of the gate electric field, such as bipolarity of the photocurrent, are described in Supplementary Section S1. The drop in photoresponse in bilayer MoS_2 also suggests that optimization of MoS_2 thickness will be required to maximize the photosensitivity and preserve the flexibility of the hybrids for eventual device applications.

In summary, graphene–MoS_2 hybrids are emerging as highly sensitive gate-tunable photodetectors and optical switches. Our recent experiments indicate that even chemical vapour deposition (CVD)-grown graphene laid on thin MoS_2 films shows these effects over a wide range of temperature, including ambient conditions (Supplementary Section S4). However, the photoresponsivity of these devices was significantly lower, presumably due to a factor of ten lower mobility of the CVD graphene used in our experiment. Nevertheless, the demonstrated remarkable stability and tunability make these promising for a new class of scalable optoelectronic memory devices.

Methods

Transfer procedure for laying graphene on MoS_2. We followed a procedure similar to that of Zomer and colleagues[30]. A piece of glass was covered with transparent tape and coated with a polymer such as poly(methyl methacrylate) (PMMA) or 9 wt% ethyl lactate (El 9). Graphene was then exfoliated onto this substrate. Separately, MoS_2 was transferred onto an Si/SiO_2 substrate by standard mechanical exfoliation and placed on the micromanipulator stage of an MJB3 mask aligner with a custom-built heater. The graphene flake, now on a transparent substrate, was positioned upside down and aligned with the MoS_2 flake using the microscope of the aligner. The two were brought into contact at an elevated temperature ($T > 100$ °C), as a result of which graphene, together with the polymer, was transferred onto the MoS_2. The polymer was later washed off with acetone.

Device fabrication and measurement. Once transferred onto MoS_2, graphene (exfoliated or CVD-grown) was etched into a desired shape by oxygen plasma. Contacts were drawn using standard electron-beam lithography, and metallization was carried out with Ti/Au (15 nm/45 nm) or Cr/Au (15 nm/45 nm). In devices where contacts were also required on the MoS_2, Au was used as the contact metal. The layout of the electrical leads was designed to measure four- or two-probe current–voltage characteristics. The devices were loaded onto a variable-temperature cryostat, and photoillumination was carried out with well-calibrated commercial LEDs through a collimating optical window. In pulsing experiments, the transient spikes in I_P following the gate pulses were removed throughout.

Quantum efficiency estimation. To calculate η we used a photoillumination power (P_{LED}) of 1 fW μm^{-2} ($\lambda = 635$ nm), which corresponds to a photon flux (Φ_P) of 3.2×10^{14} m^{-2} s^{-1}. In 1 s, I_P reached ~80% of its saturation value (Fig. 2b). At $V_g = -50$ V for the mentioned P_{LED}, $0.8 \times I_P$ corresponds to a change in V_g of 1.3 V, which can be extracted from the $I_{ds} - V_g$ curve using the scheme shown in the inset of Fig. 1b ($V_{ds} = 0.1$ V). For 285-nm-thick SiO_2, the change in carrier density (Δn) with the change in V_g (ΔV_g) can be written as $\Delta n = 7.7 \times 10^{14} \times \Delta V_g$ m^{-2}. These numbers give a quantum efficiency η of $\Phi_P/\Delta n \approx 32\%$.

Received 12 September 2012; accepted 11 September 2013; published online 20 October 2013

References

1. Novoselov, K. S. *et al.* A roadmap for graphene. *Nature* **490,** 192–200 (2012).
2. Dean, C. *et al.* Boron nitride substrates for high-quality graphene electronics. *Nature Nanotech.* **5,** 722–726 (2010).
3. Radisavljevic, B., Radenovic, A., Brivio, J., Giacometti, V. & Kis, A. Single-layer MoS_2 transistors. *Nature Nanotech.* **6,** 147–150 (2011).
4. Ghatak, S., Pal, A. N. & Ghosh, A. Nature of electronic states in atomically thin MoS_2 field-effect transistors. *ACS Nano* **5,** 7707–7712 (2011).
5. Radisavljevic, B., Whitwick, M. B. & Kis, A. Integrated circuits and logic operations based on single-layer MoS_2. *ACS Nano* **5,** 9934–9938 (2011).
6. Late, D. J., Liu, B., Matte, H. S. S. R., Dravid, V. P. & Rao, C. N. R. Hysteresis in single-layer MoS_2 field effect transistors. *ACS Nano* **6,** 5635–5641 (2012).
7. Bertolazzi, S., Krasnozhon, D. & Kis, A. Nonvolatile memory cells based on MoS_2/graphene heterostructures. *ACS Nano* **7,** 3246–3252 (2013).
8. Choi, M. S. *et al.* Controlled charge trapping by molybdenum disulphide and graphene in ultrathin heterostructured memory devices. *Nature Commun.* **4,** 1624 (2013).
9. Mak, K. F., Lee, C., Hone, J., Shan, J. & Heinz, T. F. Atomically thin MoS_2: a new direct-gap semiconductor. *Phys. Rev. Lett.* **105,** 136805 (2010).
10. Xu, X., Gabor, N. M., Alden, J. S., van der Zande, A. M. & McEuen, P. L. Photo-thermoelectric effect at a graphene interface junction. *Nano Lett.* **10,** 562–566 (2010).
11. Lemme, M. C. *et al.* Gate-activated photoresponse in a graphene p–n junction. *Nano Lett.* **11,** 4134–4137 (2011).
12. Gabor, N. M. *et al.* Hot carrier-assisted intrinsic photoresponse in graphene. *Science* **334,** 648–652 (2011).
13. Freitag, M., Low, T. & Avouris, P. Increased responsivity of suspended graphene photodetectors. *Nano Lett.* **13,** 1644–1648 (2013).
14. Tielrooij, K. J. *et al.* Photoexcitation cascade and multiple hot-carrier generation in graphene. *Nature Phys.* **9,** 248–252 (2013).
15. Biswas, C. *et al.* Negative and positive persistent photoconductance in graphene. *Nano Lett.* **11,** 4682–4687 (2011).
16. Mueller, T., Xia, F. & Avouris, P. Graphene photodetectors for high-speed optical communications. *Nature Photon.* **4,** 297–301 (2010).
17. Freitag, M., Low, T., Xia, F. & Avouris, P. Photoconductivity of biased graphene. *Nature Photon.* **7,** 53–59 (2013).
18. Echtermeyer, T. *et al.* Strong plasmonic enhancement of photovoltage in graphene. *Nature Commun.* **2,** 458 (2011).
19. Chitara, B., Panchakarla, L. S., Krupanidhi, S. B. & Rao, C. N. R. Infrared photodetectors based on reduced graphene oxide and graphene nanoribbons. *Adv. Mater.* **23,** 5419–5424 (2011).
20. Ghosh, S., Sarker, B. K., Chunder, A., Zhai, L. & Khondaker, S. I. Position dependent photodetector from large area reduced graphene oxide thin films. *Appl. Phys. Lett.* **96,** 163109 (2010).
21. Kastalsky, A. & Hwang, J. Study of persistent photoconductivity effect in n-type selectively doped AlGaAs/GaAs heterojunction. *Solid State Commun.* **51,** 317–322 (1984).
22. Nathan, M. I. Persistent photoconductivity in AlGaAs/GaAs modulation doped layers and field effect transistors: a review. *Solid State Electron.* **29,** 167–172 (1986).
23. Queisser, H. J. & Theodorou, D. E. Decay kinetics of persistent photoconductivity in semiconductors. *Phys. Rev. B* **33,** 4027–4033 (1986).
24. Dawlaty, J. M. *et al.* Measurement of the optical absorption spectra of epitaxial graphene from terahertz to visible. *Appl. Phys. Lett.* **93,** 131905 (2008).
25. Nair, R. R. *et al.* Fine structure constant defines visual transparency of graphene. *Science* **320,** 1308 (2008).
26. Konstantatos, G. *et al.* Hybrid graphene–quantum dot phototransistors with ultrahigh gain. *Nature Nanotech.* **7,** 363–368 (2012).
27. Kim, M., Safron, N. S., Huang, C., Arnold, M. S. & Gopalan, P. Light-driven reversible modulation of doping in graphene. *Nano Lett.* **12,** 182–187 (2012).
28. Sachs, B. *et al.* Doping mechanisms in graphene–MoS_2 hybrids. Preprint at http://arxiv.org/abs/1304.2236v1 (2013).
29. Britnell, L. *et al.* Strong light–matter interactions in heterostructures of atomically thin films. *Science* **340,** 1311–1314 (2013).
30. Zomer, P. J., Dash, S. P., Tombros, N. & van Wees, B. J. A transfer technique for high mobility graphene devices on commercially available hexagonal boron nitride. *Appl. Phys. Lett.* **99,** 232104 (2011).
31. Borghetti, J. *et al.* Optoelectronic switch and memory devices based on polymer-functionalized carbon nanotube transistors. *Adv. Mater.* **18,** 2535–2540 (2006).
32. Star, A., Lu, Y., Bradley, K. & Grüner, G. Nanotube optoelectronic memory devices. *Nano Lett.* **4,** 1587–1591 (2004).
33. Shi, Y. *et al.* Photoconductivity from carbon nanotube transistors activated by photosensitive polymers. *J. Phys. Chem. C* **112,** 18201–18206 (2008).
34. Dutta, S. & Narayan, K. Gate-voltage control of optically-induced charges and memory effects in polymer field-effect transistors. *Adv. Mater.* **16,** 2151–2155 (2004).

Acknowledgements

The authors acknowledge the Department of Science and Technology (DST) for a funded project under Nanomission. S.R. acknowledges support under grant no. SR/S2/CMP-02/2007 (DST).

Author contributions

K.R. and A.G. conceived and designed the experiments. K.R. and M.P. performed the experiments. K.R., M.P. and A.G. analysed the data. S.G., T.P.S. and K.R. developed the heterostructure fabrication technique used in the experiment. G.R. and S.R. contributed CVD graphene material. K.R., M.P. and A.G. co-wrote the paper. All authors discussed the results and commented on the manuscript.

Additional information

Supplementary information is available in the online version of the paper. Reprints and permissions information is available online at www.nature.com/reprints. Correspondence and requests for materials should be addressed to K.R. and A.G.

Competing financial interests

The authors declare no competing financial interests.